Data-Driven Gas Sensing Performance of Cuo Thin Films

Hussein Hassan Magli[1], Hiba Saad Rasheed[2], Shams Nassif Jassem[3],
Wathiq Ayoub Taha Al Ramdhan[4] and Rushdi Ibrahim Jasim[2]
[1]*General Directorate of Education in Al-Qadisiyah Governorate, Ministry of Education, 58001 Al-Diwaniyah, Iraq*
[2]*Department of Physics, College of Education, Mustansiriyah University, 10052 Baghdad, Iraq*
[3]*Nanotechnology and Advanced Materials Research Center, University of Technology, 10066 Baghdad, Iraq*
[4]*Department of Medical Physics, Al-Manara College for Medical Sciences, 62001 Amarah, Iraq*
rushdi77@uomustansiriyah.edu.iq
hassanhafyaa@gmail.com, hibasaad@uomustansiriyah.edu.iq, shaimaa2021@uomanara.edu.iq, wathiq.alramdhan@uomanara.edu.iq, rushdi77@uomustansiriyah.edu.iq

Keywords: Cuo, Nanostructured, CSP, Gas Sensing, Optical Properties, Sensitivity, Reactivity.

Abstract: This study investigates the synthesis and characterization of nanostructured CuO thin films deposit via chemical spray pyrolysis (CSP), emphasizing the effect of precursor solution concentrations (0.10 M, 0.15 M, and 0.20 M) on their physical properties. XRD analysis confirmed the monoclinic CuO phase with preferred (200) orientation. Increasing molarity enhanced crystallinity, as reflected by stronger diffraction peaks, larger grain sizes (17.08-19.84 nm), and reduced dislocation density and lattice strain. Morphological evaluation using AFM and SEM showed that higher molarity improved surface uniformity and reduced roughness (Rrms from 9.27 nm to 3.63 nm), with the 0.15 M film showing the most homogeneous texture. Optical analysis revealed a decrease in bandgap energy from 2.15 eV to 2.05 eV with increasing molarity, attributed to reduced quantum confinement in larger grains. All films exhibited high absorption coefficients ($>4 \times 10^4$ cm^{-1}), indicating potential for optoelectronic applications. Gas-sensing measurements demonstrated p-type semiconductor behavior, with resistance decreasing upon NO_2 exposure. The 0.20 M film achieved the highest sensitivity, around 30% greater than the 0.10 M sample-due to enhanced surface reactivity and charge transport, highlighting its suitability for gas sensor applications.

1 INTRODUCTION

In recent years, nanomaterials and nanotechnology have garnered substantial research interest owing to their size and morphology-dependent, which differ markedly from bulk materials [1], [2]. In recent years, the scientific community has shown great interest in metal oxide nanostructures owing to their extensive variety of applications and morphology-dependent properties [3], [4]. Nanostructured materials have numerous applications, including gas sensors and dye-sensitized solar cells [5], [6]. These nanomaterials are extensively employed in coatings and textile engineering due to their multifunctional antimicrobial properties, including antibacterial, antifungal, and anti-fouling capabilities [7], [8]. CuO a p-type semiconductor with a monoclinic structure has emerged as particularly noteworthy owing to its exceptional physicochemical properties and versatile applications [9]. Copper oxide (CuO) exhibits remarkable physicochemical properties, including: (i) excellent photochemical stability, (ii) high thermal resistance, (iii) economical synthesis routes, (iv) biocompatibility, (v) High-Tc superconductivity, and (vi) pronounced electrochemical activity. As a semiconductor monoxide, it features a narrow bandgap (1.2-2.1 eV) [10], [11]. Cuprous and copper oxides have been synthesized using various techniques, including CVD [12], PLD [13], thermal oxidation [14], sol-gel [15], s hydrolysis [17], electrochemically [18], [19], ion-based deposition [20], chemical conversion [21], chemical bath deposition (CBD) [22], reactive sputtering [23] and electrodeposition [24] and chemical spray pyrolysis (CSP) [25], The morphological control of copper oxide nanostructures (both CuO and Cu_2O) can be significantly enhanced through surfactant-assisted synthesis, enabling precise engineering of 2D nanosheets and 3D hierarchical architectures [26], [27]. Copper oxide nanostructures have numerous

applications across various fields. This study employed CSP to fabricate CuO nanostructures with systematically varied molar concentrations, investigating their concentration-dependent effects on physical properties.

2 EXPERIMENTAL

Copper oxide (CuO) thin films were synthesized using CSP technique, employing aqueous solutions of copper nitrate ($Cu(NO_3)_2 \cdot 6H_2O$) with varying precursor molarities of 0.10 M, 0.15 M, and 0.20 M. Each solution was magnetically stirred for 25 minutes to ensure complete homogenization before being sprayed onto pre-cleaned glass base maintained at a temperature of 350°C. The thickness of the deposited films was determined gravimetrically and found to be approximately 320 ± 25 nm. Structural characterization was carried out using XRD. Morphological features were examined using AFM to analyze surface topography. The optical properties were investigated using UV-Vis spectroscopy in the wavelength range of 300-900 nm to determine their transmittance and absorption characteristics. Gas-sensing performance was evaluated by measuring the electrical resistance of the films inside a custom-designed test chamber with dimensions of 17 cm in height and 9 cm in radius.

3 RESULTS AND DISCUSSIONS

The X-ray diffraction (XRD) analysis shown in Figure 1 reveals well-defined diffraction peaks located at 37.58°, 42.82°, and 62.36°, which are indexed to the (111), (200), and (220) crystallographic planes, respectively, in good agreement with ICDD card No. 01-075-0477. All deposited films demonstrate a preferential growth along the (200) orientation. With increasing precursor molarity, the intensity of the (200) peak becomes more pronounced, indicating enhanced crystallinity and improved grain alignment. This behavior suggests that higher molar concentrations promote more effective nucleation and crystal growth processes, leading to better structural ordering along the preferred orientation. The increase in peak intensity clearly reflects the important role of precursor concentration in controlling crystallite development and texture evolution through enhanced growth kinetics [28], [29].

The crystallite size (D) was evaluated using the standard approach reported in [31]. The calculated values, summarized in Table 1, show an increase in crystallite size from 17.08 nm to 19.84 nm with rising molar concentration. This trend indicates that higher precursor concentration supports the formation of larger crystallites. The observed enhancement in grain size can be attributed to increased nucleation density and accelerated crystal growth at higher molarity, which promotes the development of more well-defined crystalline domains [18], [30].

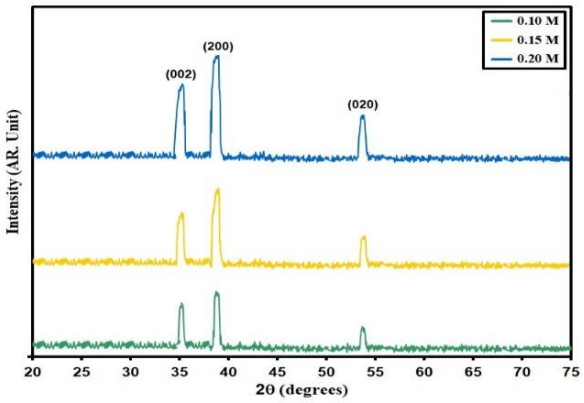

Figure 1: XRD patterns of the synthesized films.

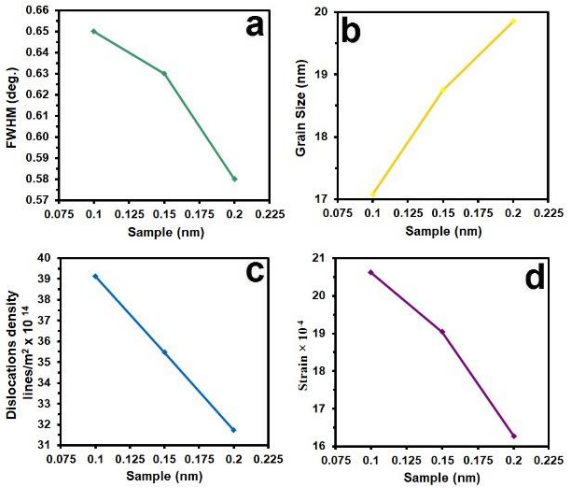

Figure 2: XRD patterns of the synthesized films.

The dislocation density (δ), which describes the density of structural defects within the crystal lattice, was determined using the relation reported in [31], [32]. The results show that δ decreases from 39.12 to 31.73 × 10^{14} lines/m² as the molar concentration increases, indicating an improvement in crystalline

Table 1: S_P, including D, E_g, and texture coefficients.

Sample (M)	2 θ (°)	(hkl) Plane	FWHM (°)	E_g (eV)	*D* (nm)	δ (× 10^{14}) (lines/m^2)	E (× 10^{-4})
0.10	38.73	200	0.65	2.15	17.08	39.12	20.62
0.15	38.70	200	0.63	2.09	18.75	35.46	19.04
0.20	38.66	200	0.58	2.05	19.84	31.73	16.28

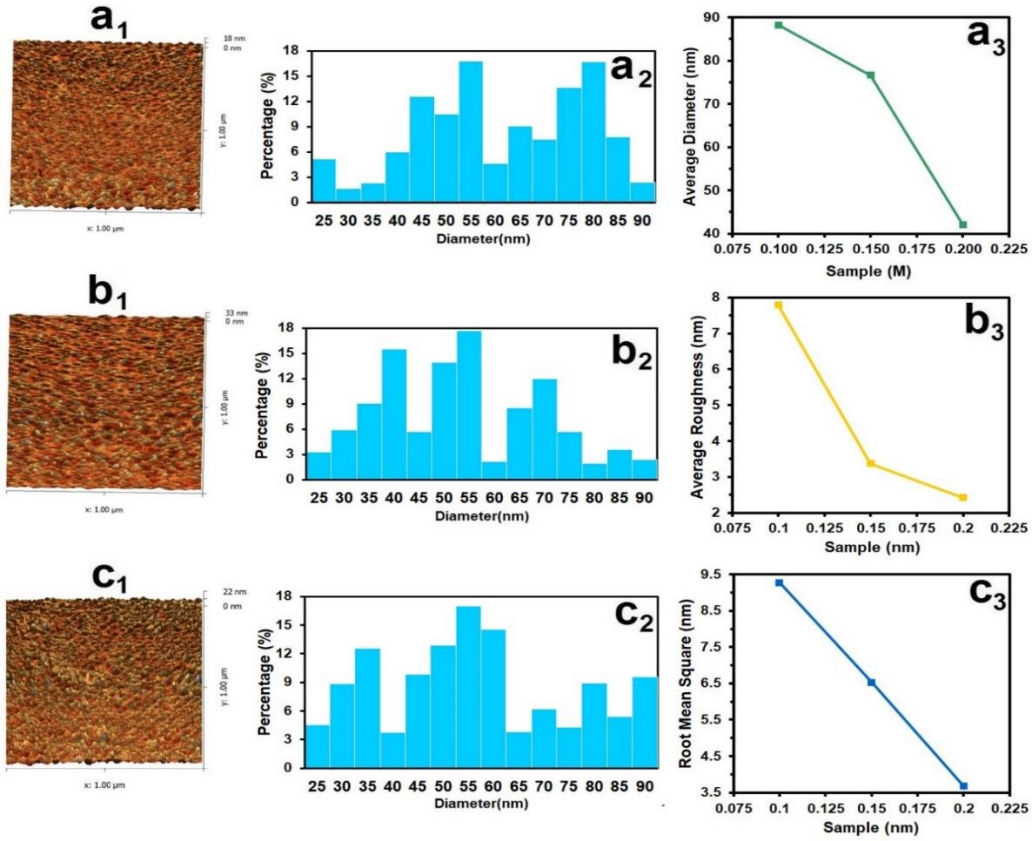

Figure 3: AFM topography images of CuO thin films prepared at different precursor molarities.

quality [10], [33]. This reduction in dislocation density suggests fewer lattice imperfections at higher concentrations. As crystallite size increases, the number of dislocations per unit volume decreases, which contributes to enhanced structural stability and improved material performance.

The lattice strain (ε), representing internal lattice distortions, was calculated based on the method described in [34], [35]. The obtained values, listed in Table 1, decrease from 30.88 × 10^{-4} to 27.50 × 10^{-4} with increasing Cd^{2+} concentration, indicating reduced structural stress and improved lattice ordering [36]. Figure 2 further illustrates the correlation between the structural parameters, showing simultaneous improvement in crystallite size, reduced dislocation density, and lower strain with increasing precursor concentration.

Figure 3 displays AFM topography images of SPT-deposited CuO films, with quantitative roughness analysis (Table 2 the AFM parameters A_{par}) showing concentration-dependent evolution of RMS and Ra values. Grain size distribution revealed a systematic decrease from 88.2 nm (0.10 M) to 42.1 nm (0.20 M), demonstrating precursor molarity's role in morphological control [37]., revealing that the average particle size (P_{av}) were approximately (88.2, 76.6 and 42.1) nm for films prepared with various molarities respectively. Notably, the RMS value decreased from 9.27 nm for the 0.10 M film to 3.63 nm as the concentration increased, indicating a smoother surface at higher molarities [14]. The

variation of Ra roughness parameters with concentration molarity is illustrated in Figures 3. Table 2 details the corresponding AFM measurement values. This decrease in surface roughness with increasing concentration molarity suggests that higher precursor concentrations promote the formation of more uniform and compact films, which can enhance the material's optical and electrical properties by reducing surface defects and scattering sites.

Table 2: A_{par} of the deposit films.

Sample (M)	P_{av} nm	R_a (nm)	RMS (nm)
0.10	88.2	7.79	9.27
0.15	76.6	3.37	6.53
0.20	42.1	2.42	3.63

Figure 4 presents the optical transmittance spectra of the films prepared using different precursor molarities (0.10 M, 0.15 M, and 0.20 M). The data indicate that all samples exhibit a wavelength-dependent decrease in transmittance, which is a typical behavior of semiconductor materials due to increased absorption at higher wavelengths. It is also observed that films synthesized at lower precursor concentrations show higher overall transparency throughout the visible region. This behavior can be explained by reduced film thickness and a lower concentration of optically active centers, which leads to diminished scattering and absorption of incident photons [38], [39].

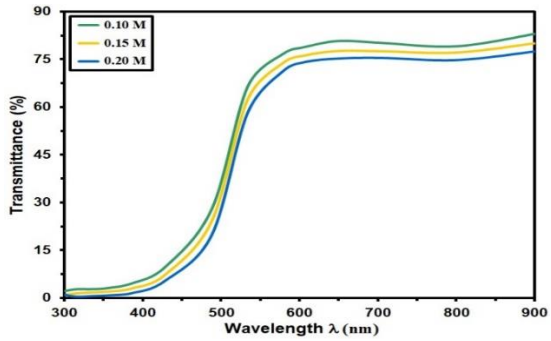

Figure 4: Transmittance of deposit films.

The absorbance (A) was evaluated from the measured transmittance using the standard optical relation reported in [40], [41], where absorbance is defined as the logarithmic inverse of transmittance. The corresponding wavelength-dependent absorbance behavior is shown in Figure 5. The results reveal that absorbance increases with increasing precursor molarity across the entire spectral range. This enhancement can be attributed to increased film thickness and improved crystallinity at higher molar concentrations, both of which enhance light–matter interaction and promote stronger photon absorption [8], [16], [42], [43].

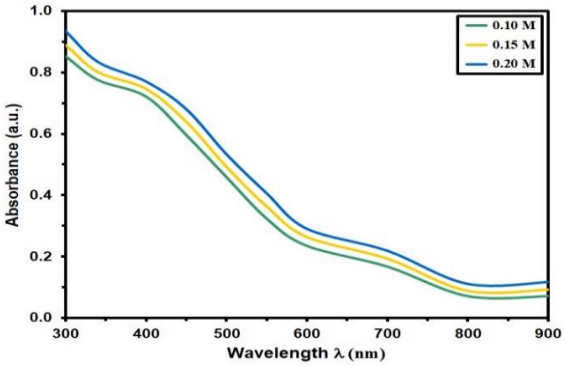

Figure 5: Absorbance of created films.

The absorption coefficient (α) was determined using the standard relation reported in [44], [45], which relates absorbance to film thickness. The obtained expression considers the influence of optical absorption within the material structure. Figure 6 illustrates the spectral variation of α as a function of wavelength for all investigated films. The results show that the absorption coefficient remains relatively high across the visible region, exceeding 4×10^4 cm^{-1} in all cases. This indicates strong light–matter interaction and confirms the suitability of the films for optoelectronic applications [12], [46].

The observed increase in absorption coefficient can be linked to improvements in crystallinity and a reduction in defect density as precursor molarity increases. In particular, larger crystallite sizes and fewer structural imperfections enhance the efficiency of photon absorption, while reduced defect-related scattering further contributes to higher optical response. Overall, the improvement in structural quality with increasing molarity leads to more efficient absorption behavior [48].

The optical bandgap (Eg) was evaluated using the Tauc relation for direct transitions as described in [47], [48]. The corresponding plots of $(\alpha h\nu)^2$ versus photon energy ($h\nu$) are shown in Figure 7. The results indicate a gradual decrease in Eg with increasing precursor molarity. The estimated bandgap values are 2.15 eV, 2.09 eV, and 2.05 eV for 0.10 M, 0.15 M, and 0.20 M, respectively, consistent with previously reported values for CuO thin films prepared by various techniques [49], [50]. This reduction in bandgap is attributed to increased crystallite size and reduced defect concentration at higher molarity. As

grain size increases, quantum confinement effects become weaker, leading to a narrowing of the bandgap and modification of the electronic structure [19].

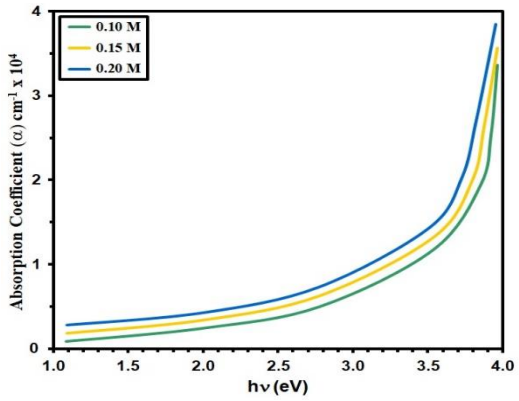

Figure 6: α for the prepared films.

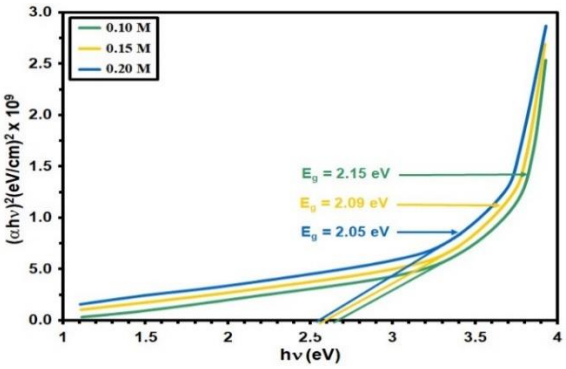

Figure 7: $(\alpha h\nu)^2$ versus hν of the prepared films.

The extinction coefficient (k), which describes the attenuation of electromagnetic radiation as it propagates through the material, was determined using the relation reported in [51], [52]. In this expression, λ denotes the wavelength. The spectral dependence of k is presented in Figure 8, which shows that the extinction coefficient decreases with decreasing precursor molarity [53], [54]. This behavior suggests that films deposited at lower molar concentrations experience reduced optical losses, indicating weaker absorption and scattering of incident light.

The reduction in k can be associated with variations in film microstructure, including changes in thickness, crystallinity, and defect density. In particular, lower extinction coefficients imply a more uniform surface with fewer structural imperfections, which contributes to improved optical transparency and reduced attenuation of electromagnetic waves.

The refractive index (n) was evaluated using the relation given in [55], [56], where reflectance is the key optical parameter. The variation of n with precursor molarity is shown in Figure 9. The results indicate that the refractive index decreases as molarity increases [18], [57]. This trend can be explained by microstructural modifications induced by changes in precursor concentration. Higher molarity tends to enhance crystallinity and grain growth, which can modify packing density and porosity, ultimately affecting how light propagates through the film and resulting in a lower refractive index.

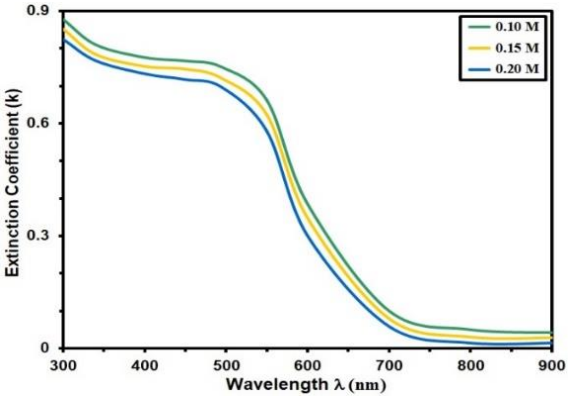

Figure 8: k of the deposit films.

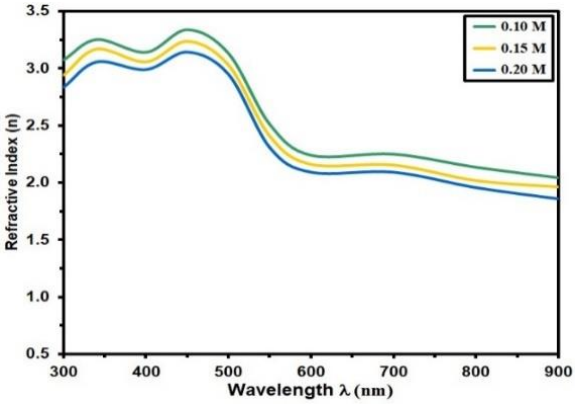

Figure 9: n of created films.

Figure 10 illustrates the dynamic resistance response of CuO thin films to NO_2 gas at 125 °C. All samples exhibit a decrease in resistance upon gas exposure, confirming p-type semiconducting behavior [58], [59]. This response arises from the interaction between NO_2 molecules and the film surface, where NO_2 acts as an electron-accepting species, extracting electrons from the conduction band and increasing hole concentration, which leads

to reduced resistance [57]–[59]. Among all samples, the film prepared at 0.20 M shows the highest baseline resistance and the strongest sensing response, indicating that precursor concentration significantly influences both structural and electronic properties [60], [61]. Quantitatively, the 0.20 M film exhibits approximately 25% higher response amplitude and about 40% higher baseline resistance compared to the 0.10 M film, which is attributed to enhanced surface reactivity and improved charge transport properties [62], [63].

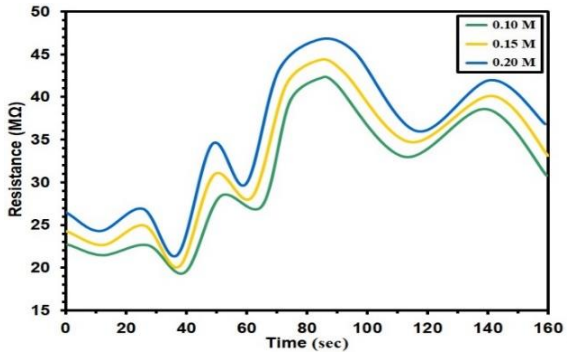

Figure 10: Resistance of the created films.

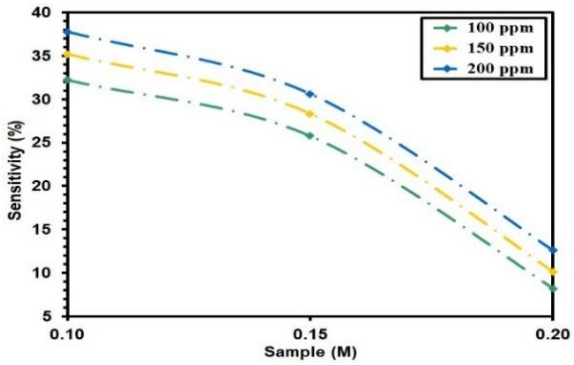

Figure 11: Sensitivity of the deposit films.

The gas sensing response (sensitivity) was evaluated using the standard relation given in [64], [65], which expresses the relative change in resistance upon exposure to the target gas. Figure 11 presents the NO_2 sensitivity of CuO thin films prepared at different precursor molarities (0.10–0.20 M) over a concentration range of 100–200 ppm. The results show that sensitivity increases with increasing NO_2 concentration for all samples, demonstrating a clear concentration-dependent behavior. Among the studied films, those prepared at 0.20 M exhibit approximately 30% higher sensitivity compared to the 0.10 M films, confirming the strong influence of precursor molarity on gas sensing performance [40]. The maximum sensitivity is observed at 200 ppm for the 0.20 M sample, indicating its superior sensing efficiency [66], [67].

4 CONCLUSIONS

This study successfully synthesized and characterized nanostructured CuO thin films using the CSP, focusing on the effect of molar concentrations on their properties. XRD analysis confirmed the monoclinic CuO phase with a preferred (200) orientation. Higher molarity enhanced crystallinity, increased grain size (17.08-19.84 nm), and reduced dislocation density and lattice strain. AFM and SEM analyses showed that increasing precursor concentration led to smoother surfaces (Rrms reduced from 9.27 nm to 3.63 nm) and more uniform grain distribution. The 0.15 M sample displayed the most homogeneous morphology, while the 0.20 M sample exhibited flake-like features. Optical measurements revealed a bandgap reduction from 2.15 eV to 2.05 eV with increasing molarity, attributed to reduced quantum confinement. All films showed high absorption coefficients (>4 x 10^4 cm^{-1}). Gas-sensing tests confirmed p-type behavior with improved sensitivity at higher molarity. The 0.20 M film showed 30% higher sensitivity than the 0.10 M film, making it ideal for sensing applications.

ACKNOWLEDGMENTS

Financial support from Mustansiriyah University is gratefully acknowledged.

REFERENCES

[1] U.C. Bind and R.K. Dutta, et al., “Ion implantation induced phase transformation and enhanced crystallinity of copper oxide thin films,” Superlattices Microstruct., vol. 84, pp. 24-35, 2015.

[2] D. Arunkumar, P. Francis and J. Merlineshyla, Arch. Appl. Sci. Res., vol. 4, p. 2174, 2012.

[3] N.M. Basith, J.J. Vijaya, L.J. Kennedy and M. Bououdina, “Structural, morphological, optical and magnetic properties of Ni-doped CuO nanostructures,” Mater. Sci. Semicond. Process., vol. 17, pp. 110-118, 2014.

[4] I. Erdogan and O. Gullu, “Optical and structural properties of CuO nanofilm: its diode application,” J. Alloys Compd., vol. 492, pp. 378-383, 2010.

[5] E.M. Alkoy and P.J. Kelly, “,” Vacuum, vol. 79, p. 221, 2005.

[6] T. Maruyama, “Copper oxide thin films prepared by chemical vapor deposition,” Sol. Energy Mater. Sol. Cells, vol. 56, no. 1, pp. 85-92, 1998.

[7] G. Papadimitropoulos, N. Vourdas, V. Vamvakas and D. Davazoglou, “,” J. Phys. Conf. Ser., vol. 10, p. 182, 2005.

[8] V. Saravanan, P. Shankar, et al., “Growth and characterization of copper oxide thin films,” J. Anal. Appl. Pyrolysis, vol. 111, pp. 272-277.

[9] A.N. Tuama, K.H. Abbas, M.Q. Hamzah, S.O. Mezan, A.H. Jabbar and M.A. Agam, “An overview on characterization of Ag/Cu2O nanometallic,” Int. J. Adv. Sci. Technol., vol. 29, no. 3, pp. 5008-5018, 2020.

[10] E. Vigil, F.A. Fernandez-Lima, J.A. Ayllon, E. Pedrero, I. Zumeta, B. Gonzalez, L. Curbelo, H.D. Fonseca-Filho, M.E.H. Maia da Costa, C. Domingo, M. Behar and F.C. Zawislak, “,” Microporous Mesoporous Mater., vol. 109, p. 560, 2008.

[11] A.A. Jalil, et al., “Tailoring the current density to enhance photocatalytic activity of CuO,”J. Electroanal. Chem., vol. 701, pp. 50-58, 2013.

[12] W. Seiler, E. Millon, J. Perriere, R. Benzerga and C. Boulmer-Leborgne, “Epitaxial growth of copper oxide films,” J. Cryst. Growth, vol. 311, pp. 3352-3358, 2009.

[13] X. Jiang, T. Herricks and Y. Xia, “CuO nanowires synthesis by heating copper,” Nano Lett., vol. 2, no. 12, pp. 1333-1338, 2002.

[14] Y.K. Su, et al., “Controlled synthesis of CuO nanowire arrays,” J. Alloys Compd., vol. 17, no. 4, p. 783, 2007.

[15] J. Zhu, et al., “Synthesis of flower-like CuO nanostructures,” Mater. Lett., vol. 61, no. 30, p. 5236, 2007.

[16] G.Q. Yuan, et al., “Electrochemical synthesis of CuO nanocrystals,” J. Cryst. Growth, vol. 303, no. 2, p. 400, 2007.

[17] L. Yu, et al., “CuO nanoflowers synthesis and field emission,” J. Cryst. Growth, vol. 310, no. 12, p. 3125, 2008.

[18] K.H. Yoon, W.J. Choi and D.H. Kan, “Photoelectrochemical properties of copper oxide thin films,” Thin Solid Films, vol. 372, pp. 250-256, 2000.

[19] P. Richharia, K.L. Chopra and M.C. Bhatnagar, “Surface analysis of copper selective coating,” Sol. Energy Mater., vol. 23, no. 1, pp. 93-109, 1991.

[20] N. Saadaldin, M.N. Alsloum and N. Hussain, “Preparation of copper oxide thin films by CBD,” vol. 74, pp. 1459-1465, 2015.

[21] V. Rajendran and J. Gajendiran, “Preparation of nanocrystalline CuO powders,” Mater. Res. Bull., vol. 56, pp. 134-137, 2014.

[22] W.T. Yao, et al., “Formation of uniform CuO nanorods,” J. Phys. Chem. B, vol. 109, no. 29, p. 14011, 2005.

[23] Y. Liu, et al., “Synthesis of copper oxide nanocrystals,” J. Mater. Chem., vol. 16, no. 2, p. 192, 2006.

[24] J. Morales, L. Sánchez, F. Martín, J.R. Ramos-Barrado and M. Sánchez, “Use of CuO thin films in lithium cells,” Thin Solid Films, vol. 474, no. 1-2, pp. 133-140, 2005.

[25] B. Balamurugan and B.R. Mehta, “Optical and structural properties of CuO films,” Thin Solid Films, vol. 396, no. 1, pp. 90-96, 2001.

[26] N. Serin, T. Serin, S. Horzum and Y. Celik, “Annealing effects on copper oxide films,” Semicond. Sci. Technol., vol. 20, pp. 398-401, 2005.

[27] J.I. Pankove, Optical Processes in Semiconductors, New Jersey, NJ, USA: Prentice Hall, 1971.

[28] A.A. Ogwu, E. Bouquerel, O. Ademosu, S. Moh, E. Crossan and F. Placido, “Influence of rf power on CuO films,” J. Phys. D, vol. 38, p. 266, 2005.

[29] G. Papadimitropoulos, N. Vourdas, E. Vamvakas and D. Davazoglou, “Optical and structural properties of copper oxide thin films,” Thin Solid Films, vol. 515, pp. 2428-2432, 2006.

[30] R.S. Ali, H.S. Rasheed, N.F. Habu bi and S.S. Chiad, “Synthesis and characterization of Mn-doped FeS2 thin films,” Chalcogenide Lett., vol. 20, no. 1, pp. 63-72, 2023.

[31] K. Phiwdang, et al., “Synthesis of CuO nanoparticles by precipitation method,” Energy Procedia, vol. 34, pp. 740-745, 2013.

[32] M.B. Jumaa, T.H. Mubarak and A.M. Mohammad, “Structural and magnetic properties of nanoferrites,” AIP Conf. Proc., vol. 2475, 090014, 2023.

[33] S.K. Muhammad, E.S. Hassan, K.Y. Qader, K.H. Abass, S.S. Chiad and N.F. Habubi, “Effect of vanadium on SnO2 thin films,” Nano Biomed. Eng., vol. 12, no. 1, pp. 67-74, 2020.

[34] J. Zhu, et al., “Highly dispersed CuO nanoparticles,” Mater. Lett., vol. 58, pp. 3324-3327, 2004.

[35] H.A. Hussin, R.S. Al-Hasnawy, R.I. Jasim, N.F. Habubi and S.S. Chiad, “Optical and structural properties of CuO thin films doped by Mn,” J. Green Eng., vol. 10, no. 9, pp. 7018-7028, 2020.

[36] K. Mageshwari and R. Sathyamoorthy, “Synthesis of CuO microspheres,” Appl. Nanosci., vol. 3, pp. 161-166, 2013.

[37] F. Wang, et al., “Gas sensor based on CuO nanoparticles,” RSC Adv., vol. 6, no. 83, pp. 79343-79349, 2016.

[38] M.A. Dar, et al., “Structural and magnetic properties of CuO nanoneedles,” Appl. Surf. Sci., vol. 254, pp. 7477-7481, 2008.

[39] O.V. Abramov, et al., “Sonochemical coating of nanoparticles,” Surf. Coat. Technol., vol. 204, pp. 718-722, 2009.

[40] M.H. Yamukyan, K.V. Manukyan and S.L. Kharatyan, “Copper oxide reduction,” J. Chem. Eng., vol. 137, pp. 636-642, 2008.

[41] Z. Yang, et al., “Gas-sensing properties of CuO microspheres,” Sens. Actuators, vol. 128, pp. 293-298, 2007.

[42] Y. Xu, D. Chen and X. Jiao, “Fabrication of CuO microspheres,” J. Phys. Chem. B, vol. 109, pp. 13561-13566, 2005.

[43] Y. Zhang, et al., “CuO nanocrystals synthesis,”J. Cryst. Growth, vol. 291, pp. 196-201, 2006.

[44] J. Wang, et al., “Synthesis of CuO nanocrystals,”J. Chem. Sci., vol. 121, pp. 1077-1081, 2009.

[45] A.A. Kamil, N.A. Bakr, T.H. Mubarak and J. Al-Zanqanawee, “Synthesis of Au and Ag nanoparticles,” Dig. J. Nanomater. Biostruct., vol. 16, no. 4, pp. 1219-1226, 2021.

[46] H.S. Al-Rikabi, M.H. Al-Timimi and W.H. Albanda, "Morphological and optical properties of MgO-ZnS films," Dig. J. Nanomater. Biostruct., vol. 17, no. 3, pp. 889-897, 2022.

[47] E.S. Hassan, A.K. Elttayef, S.H. Mostafa, M.H. Salim and S.S. Chiad, "Silver oxide nanoparticles in gas sensors," J. Mater. Sci. Mater. Electron., vol. 30, no. 17, pp. 15943-15951, 2019.

[48] S.K. Maji, et al., "Chemical synthesis of mesoporous CuO," J. Solid State Chem., vol. 183, pp. 1900-1904, 2010.

[49] C.Y. Huang, et al., "Photoluminescence properties of CuO nanowire," Appl. Surf. Sci., vol. 256, pp. 3688-3692, 2010.

[50] H. Siddiqui, M.S. Qureshi and F.Z. Haque, "Hydrothermal synthesis of CuO tetrapods,"Optik, vol. 125, pp. 4663-4667, 2014.

[51] M.A. Vila, C. Diaz-Guerra and J. Piqueras, "Optical and magnetic properties of CuO nanowires,"J. Phys. D, vol. 43, 135403, 2010.

[52] B.A. Bader, S.K. Muhammad, A.M. Jabbar, K.H. Abass, S.S. Chiad and N.F. Habubi, "Indium-doped CdO thin films," J. Nanostruct., vol. 10, no. 4, pp. 744-750, 2020.

[53] A.S. Lanje, et al., "Synthesis and optical characterization of CuO nanoparticles," Adv. Appl. Sci. Res., vol. 2, pp. 36-40, 2010.

[54] M. Chang, H. Liu and C.Y. Tai, "Preparation of CuO nanoparticles," Powder Technol., vol. 207, pp. 378-386, 2011.

[55] E.H. Hadi, M.A. Abbsa, A.A. Khadayeir, Z.M. Abood, N.F. Habubi and S.S. Chiad, "Effects of Mn doping on TiO2 thin films," J. Phys.: Conf. Ser., vol. 1664, 2020.

[56] C.L. Carnes and K.J. Klabunde, "Catalytic methanol synthesis," J. Mol. Catal. A, vol. 194, pp. 227-236, 2003.

[57] S. Anandan, X. Wen and S. Yang, "Growth of CuO nanorod arrays," Mater. Chem. Phys., vol. 93, pp. 35-40, 2005.

[58] P. Chand and P. Kumar, "Effect of precursors on CuO nanostructures," Optik, vol. 156, pp. 743-753, 2018.

[59] J.R. Lakowicz, Fluorescence Spectroscopy, Boston, MA, USA: Springer, 1983.

[60] K. Mageshwari, R. Sathyamoorthy and J. Park, "Photocatalytic activity of CuO microspheres," Powder Technol., vol. 278, pp. 150-156, 2015.

[61] P. Mallick and S. Sahu, "Optical absorption of CuO nanoparticles," Nanosci. Nanotechnol., vol. 2, pp. 71-74, 2012.

[62] N.C. Horti, et al., "Photoluminescence properties of SnO2 nanoparticles," Optik, vol. 169, pp. 314-320, 2018.

[63] H. Siddiqui, M.S. Qureshi and F.Z. Haque, "Wet chemical synthesis of CuO nanostructures," Optik, vol. 127, pp. 2740-2747, 2016.

[64] R.I. Jasim, E.H. Hadi, S.S. Chiad, N.F. Habubi, M. Jadan and J.S. Addasi, "Effect of silver doping on CdSe thin films," J. Ovonic Res., vol. 19, no. 2, pp. 187-196, 2023.

[65] K.J. Muthe, Vyas, S. Narang, D. Aswal, S. Gupta, D. Bhattacharya, R. Pinto, G. Kothiyal and S. Sabharwal, "CuO phase formation during thin film deposition," Thin Solid Films, vol. 324, pp. 37-43, 1998.

[66] S.A. Sadeq, et al., "Copper oxide nanomaterial saturable absorber," Results Phys., vol. 10, pp. 264-269, 2018.

[67] S. Raja and M. Deepa, "Synthesis of polyaniline-copper oxide nanocomposite," Ind. J. Adv. Chem. Sci., vol. 3, pp. 198-203, 2015.